Journal Pre-proof

Ecoflex polymer of different Shore hardnesses: Experimental investigations and constitutive modelling

Zisheng Liao, Mokarram Hossain, Xiaohu Yao

PII: S0167-6636(20)30020-X
DOI: https://doi.org/10.1016/j.mechmat.2020.103366
Reference: MECMAT 103366

To appear in: *Mechanics of Materials*

Received date: 6 January 2020
Revised date: 10 February 2020
Accepted date: 15 February 2020

Please cite this article as: Zisheng Liao, Mokarram Hossain, Xiaohu Yao, Ecoflex polymer of different Shore hardnesses: Experimental investigations and constitutive modelling, *Mechanics of Materials* (2020), doi: https://doi.org/10.1016/j.mechmat.2020.103366

Highlights

- A thorough experimental characterization of Ecoflex polymer of five Shore hardnesses
- Strain rate and temperature influences are analysed
- Stress softening and recovery behaviour have been identified
- Shore-dependent constitutive models are developed
- A pseudo-softening model is coupled with Shoredependent

Ecoflex polymer of different Shore hardnesses: Experimental investigations and constitutive modelling

Zisheng Liao[a,b,c], Mokarram Hossain[b,*], Xiaohu Yao[a,c,*]

[a]*School of Civil Engineering and Transportation, South China University of Technology, 510640 Guangzhou, Guangdong, China*
[b]*Zienkiewicz Centre for Computational Engineering, College of Engineering, Swansea University, SA1 8EN, United Kingdom*
[c]*State Key Laboratory of Subtropical Building Science, South China University of Technology, Guangzhou 510640, China*

Abstract

Ecoflex, a commercially available silicone polymer, has attracted considerable attention due to its wide range of applications. The polymer has various Shore hardnesses that represent its wide range of stiffnesses. In this contribution, we have conducted a plethora of experiments under the uniaxial mode of tensile deformation. These experiments consist of loading-unloading cyclic tests, stretchability tests, single-step relaxation tests, Mullins effect tests, stress recovery tests, and temperature-dependence tests at different strain levels. All tests are revisited with Ecoflex of five Shore hardnesses ranging from Shore 00-10 to Shore 00-50. Extensive experimental findings illustrate that the material consists of an equilibrium stress part and an overstress part. Constitutive frameworks with an amplified strain invariant are proposed to predict the mechanical responses of Ecoflex over a wide range of Shore hardnesses. Afterwards, the frameworks are extended to capture the stress softening behaviour significantly observed in the material. Relevant examples illustrate that proposed constitutive models accurately predict stress-strain responses and the stress softening behaviour of Ecoflex. The current experimental study will work as a guide in selecting Ecoflex with an appropriate Shore hardness for applications in stretch sensors, soft robotics, and energy harvesters. Moreover, the novel concept of Shore-dependent modelling proposed herein can be applied to predict the stress-strain behaviour of other soft polymers appearing with various Shore hardnesses where there exist difficulties in obtaining experimental data of a particular Shore hardness.

Keywords: Ecoflex silicone rubber, Stress softening, Shore hardness, Constitutive model, Strain invariant amplification

1. Introduction

Polymers, particularly rubber-like materials, become indispensable parts of everyday life. Among other rubber-like materials, silicone elastomers are crucial ingredients in recent years. They have various exotic and promising properties such as bio-compatibility, non-toxicity, good transparency, thermal stability, climate, oxidative, and ultra-violet (UV) resistance. Out of the aforementioned properties, good biocompatibility and relatively inert actions with chemicals make silicones as one of the most used materials in biomedical engineering in forms of tubing, peristaltic pumps, catheters and various cardiovascular devices

*Corresponding authors
Email addresses: l.zisheng@mail.scut.edu.cn (Zisheng Liao), mokarram.hossain@swansea.ac.uk (Mokarram Hossain), yaoxh@scut.edu.cn (Xiaohu Yao)

such as heart pumps, ventricular assist devices, cannulas and vascular grafts [1, 2, 3, 4]. Silicones have stiffnesses that are very matchable to biological tissues. Therefore, many of them have been used for skin-like applications or external maxillofacial prosthetics [5]. Not limited to biomedical engineering, silicones are also the key materials in the recently emerging soft robotics [6, 7, 8]. Wearable and flexible stretch-sensors become emerging sectors for healthcare applications, cf. [9, 10, 11, 12, 13, 14]. Furthermore, actuating materials in soft robotics and flexible rubber-like materials for energy harvesting from ambient motions such as human walking and ocean and tidal waves are also current areas of active research where appropriate soft and flexible materials have great demands [15, 16]. Thanks to many favourable rheological and mechanical properties such as low viscosity, high reproducibility, large deformability, and low sensitivity to temperature, silicone-inspired filled polymers are major candidates in the aforementioned recent areas. Moreover, due to low dissipative behaviour and low leakage characteristics, silicones and their composites have been increasingly applied in aerospace industries [17].

Ecoflex^{TM} (Smooth-On, USA) is a commercially available rubber-like material that comes up with several Shore hardnesses ranging from Shore 00-10 to Shore 00-50. The material has very low viscosity with a reasonable curing time (four hours) which can be stretched many times its original size without tearing and will rebound to its original form without distortion. Wearable stretch sensors for epidermal electronic systems require mechanical compliance like human skin and a high stretchability, where Ecoflex and other soft silicones become ideal candidates. Very recently, in an effort to develop highly sensitive, largely stretchable, ultra-soft and skin-mountable strain sensors, Amjadi et al. [9] used Ecoflex-carbon nanotube nanocomposite thin films. In this case, single-walled carbon nanotubes hugely enhance the sensing capability of Ecoflex matrix, where the latter provides good linearity and small drift at different strain levels and stain rates. In contrast to Amjadi et al. [9], Mai et al. [11] manufactured self-standing piezoresistive sensors by blending multiwall carbon nanotubes with Ecoflex. Such composite sensors showed a low electrical percolation threshold of 0.3 wt%, with an elastic modulus as soft as the human skin in the forearm and palm dermis. More works in the area of stretch-based sensors using Ecoflex as a matrix material are due to Jiang et al. [14], Kim et al. [12], Lee et al. [13]. Another important application of Ecoflex is related to tissue biomechanics. A prolonged mechanical loading disrupts blood flow and metabolic clearance inside a human body and therefore it causes deep tissue injury. Sparks et al. [18] conducted unconfined compression experiments on two different Shore hardnesses of Ecoflex (00-30 and 00-10) in an effort to mimic stress and strain in deep muscle tissues.

Previous experimental investigations related to Ecoflex are very limited. Steck et al. [19] examined the nonlinear elastic response of Ecoflex under both compressible and incompressible constraints. They found that under uniaxial tensile tests, Ecoflex shows slight compressibility which increases with stretching. Based on the experimental study, they further considered five classical hyperelastic models to describe the nonlinear elastic responses of the polymer under both compressible and incompressible conditions. However, all of the tests conducted in their study were performed at a fixed strain rate. Furthermore, the study only considered Ecoflex of Shore hardness 00-30. To the best of the authors' knowledge, a systematic thermo-viscoelastic experimentation to quantify this soft material, as well as its constitutive model that can predict the mechanical behaviour with different Shore hardnesses, are absent in the literature. Hence, in this contribution, we perform loading-unloading-reloading cyclic tests at different strain rates and strain levels, single-step relaxation tests with various strains and holding time, stress softening tests for identifying Mullins effect, etc on various Shore hardnesses. Based on the experimental results, a constitutive model is proposed which can predict stress-strain responses of Ecoflex of different Shore hardnesses including equilibrium response and

Figure 1. A complete thermo-viscoelastic testing system: ① is the main framework of the Instron 5567, ② is the control computer, ③ is the temperature chamber, ④ is the force sensor to monitor the applied force, and ⑤ is the crosshead of ①.

stress softening behaviour.

The paper is organised as follows: Sec. 2 elaborates the experimental set-up, procedures for sample preparations which are utilised to perform the experiments in our laboratory. In the following section Sec. 3, comprehensive experimental results are illustrated in detail, and sufficient analyses are given. In these cases, cyclic and relaxation behaviour, stress softening and recovery of Ecoflex are extensively analysed. Furthermore, the strain rate and temperature dependences of the polymer are investigated and explained in the same section. Sec. 4 illustrates a novel way to model hyperelastic responses of Ecoflex of different Shore hardnesses which is further extended to capture the stress softening behaviour of the material in the same section. Sec. 5 describes a parameter identification procedure and then the model is validated using the data appearing in the previous section.

2. Experimental set-up and sample preparations

In this contribution, Ecoflex rubbers of four Shore hardnesses, e.g., 00-10, 00-20, 00-30, and 00-50 have been selected for experimental investigations. For model validation purposes, some complementary tests on Shore 00-35 are also carried out. Note that except Shore 00-35, the curing time of the polymers is about four hours. However, the curing time of Ecoflex Shore 00-35 lasts only for a few minutes. Therefore, it is difficult to produce good specimens for this Shore manually within a very short span of curing time. Ecoflex rubbers are two-component platinum-catalyzed room-temperature curable silicones. Two liquid parts of each Shore hardness are mixed and stirred manually with a 1:1 ratio, and the liquid mixture is then injected with a syringe into a 3D printed customized mould. For uniaxial experimentations, rectangular specimens with 50 mm $\times$ 5 mm $\times$ 1 mm (length $\times$ width $\times$ thickness) are adopted. A similar dimension is taken for the uniaxial tensile experimental investigations of various soft polymers, see [20, 21, 22, 23, 24]. The semi-finished specimens are then degassed in a vacuumiser to guarantee the removal of trapped air bubbles. After holding an overnight (beyond the recommended four-hour curing time in the specification supplied by the manufacturer), specimens are demoulded smoothly. In an attempt to avoid the slippage due to the extreme softness and stretchability, each specimen is adhered to plastic slices by silicone glues in both ends,

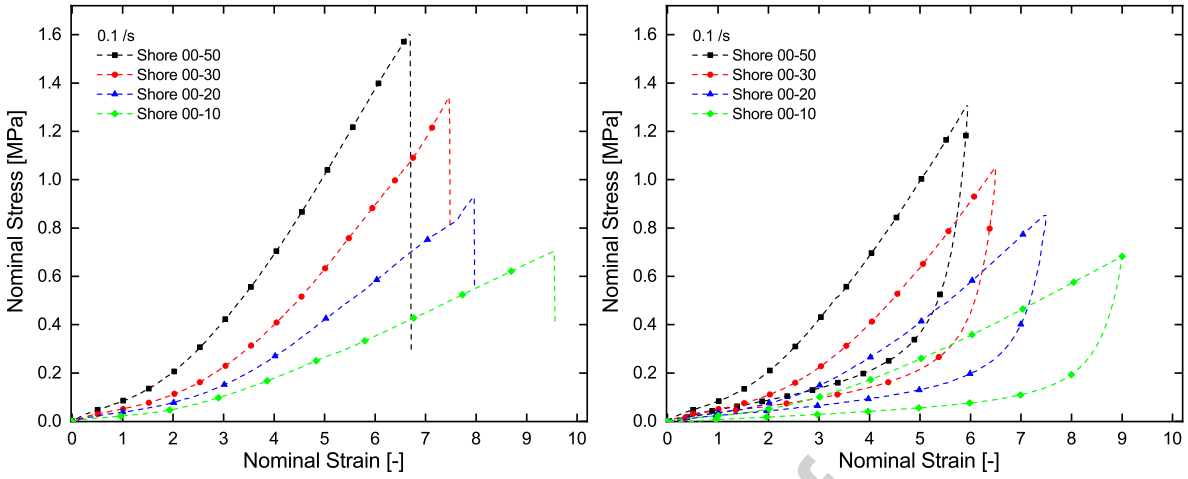

Figure 2. (a) Stretchability tests on specimens of different Shore hardnesses, (b) cyclic tests at large deformation before failure of different Shore hardnesses.

Figure 3. A typical specimen after being stretched to fail; a failure usually occurs in the middle

see Fig. 3.

For extensive and systematic experimental characterizations on Ecoflex, an Instron 5567 Universal Test Machine is used, as is shown in Fig. 1. A force sensor (④ in Fig. 1) of ±50 N maximum capacity with a precision of 0.001 N is attached to the frame. The maximum loading speed of the machine crosshead (⑤ in Fig. 1) is 8 mm/s. The displacement limit of the machine without using the temperature chamber is 800 mm. Inside the chamber, the displacement is confined to 200 mm. A Bluehill® universal user interface software on the control computer (② in Fig. 1) is utilized to interact with the machine and to extract experimental data for further analyses.

3. Experimental results

In this paper, all stress calculations are presented in the form of the so-called first Piola (nominal) stress (i.e., the applied force divided by the initial undeformed cross-sectional area) against the corresponding nominal strain (i.e., the deformation divided by the initial length of a specimen). Strain rates, mentioned throughout the contribution, are the time derivative of the nominal strains. In order to ensure the reproducibility, more than three specimens are used for each test condition. In the section follows, thermo-viscoelastic mechanical behaviour of Ecoflex will be discussed in details.

Table 1: Summary from cyclic tests : ultimate elongation at break, total and dissipation energy densities of four Shore hardnesses.

Shore hardness	Strain [-]	Total energy density [MPa]	Dissipation energy density [MPa]
00-10	9.0	2.33	1.56
00-20	7.5	2.27	1.27
00-30	6.5	2.35	1.28
00-50	6	2.97	1.70

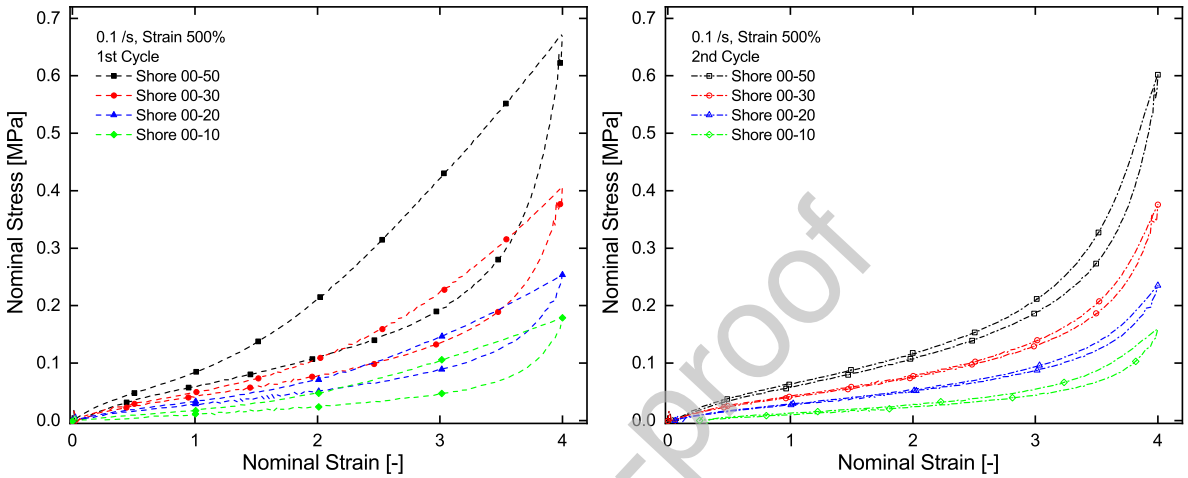

Figure 4. Cyclic tests on different Shore hardnesses of Ecoflex specimens at 400% strain. (a) The first cycles, (b) the second cycles.

3.1. *Stretchability of Ecoflex*

In an effort to understand the deformability of Ecoflex of different Shore hardnesses, a number of tensile tests are performed on each Shore, as is shown in Fig. 2(a). As expected, with the increase of the Shore hardness, on the one hand, the stretchability of Ecoflex is decreasing. On the other hand, an Ecoflex of higher Shore results in a higher strength. During experiments, it was observed that most of the specimens break in the middle instead of at the end close to the gripper, as is shown in Fig. 3. These results exclude the influence of gripper in the failure point. It can be concluded, in general, that a higher Shore hardness Ecoflex possesses a larger strength but a shorter ultimate elongation at break, cf. Fig. 2(a). This observation is similar to other soft polymers such as Polyurethanes as described in [25, 26]. In addition to tensile tests, a couple of loading-unloading cyclic tests on different Shore hardnesses before failure are also conducted, as is shown in Fig. 2(b). Note that the failure point varies from specimen to specimen due to several unavoidable reasons, such as trapped bubbles, variations in sample placements in the machine, clamping of samples, etc. Nevertheless, the energy density near failure are at a similar level, see Tab. 1. There is a possibility that the failure depends on the energy consumed regardless of the Shore hardness.

3.2. *Cyclic and stress softening behaviour*

In order to quantify the dissipative behaviour of the material, several loading-unloading cyclic tests are performed at a fixed strain rate of 0.1 /s on samples of different Shore hardnesses. As is shown in Fig. 4, an

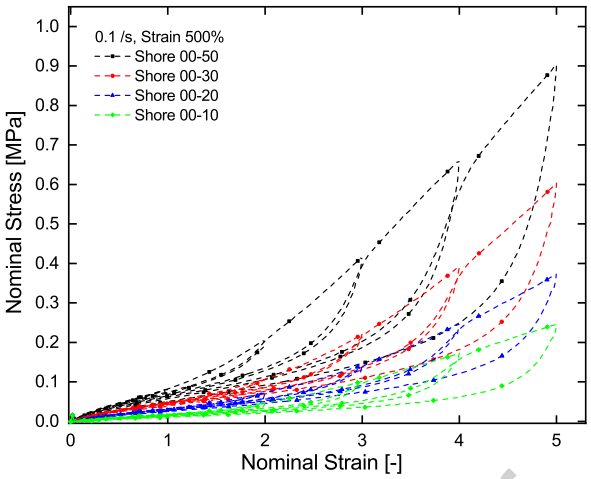

Figure 5. Multi-cycle tests with increasing strain levels on different Shore hardnesses specimens up to 500% strain.

Ecoflex of higher Shore hardness exhibits greater stiffness and larger hysteresis. This type of increased dissipative behaviour is very similar to particle-filled polymers of increasing volume fractions [27, 28]. If we compare the first and the second cycles on each Shore hardness, it is clear that there exists a significant stress softening as the hysteresis reduces significantly after the first cycle. Most of the stress softening, which is characterized by a lower resulting stress for the same applied strain, appears after the first loading cycle.

For illustrating the material softening resulting from the so-called Mullins effect, cyclic tensile tests with increasing stretches after the first cycles are performed on Ecoflex of various Shore hardnesses. In Fig. 5, it can be seen that when the applied stretch exceeds the maximum extension previously applied, the material stress-strain response returns on the same unloading path of the first cycle. That means the curves of the loading-unloading tests of virgin specimens in Fig. 4(a) serve as envelopes of the multi-cycle tests on all Shore hardnesses. This is a typical feature of the Mullins effect [29, 30, 31, 32, 33, 28]. Therefore, it can be concluded that Ecoflex, despite being an unfilled rubber, shows a significant Mullins effect.

3.3. Stress relaxation behaviour

Stress relaxation is one of the key characteristics of viscoelastic soft polymers. The understanding of the stress relaxation behaviour of soft materials is very important, particularly in the applications of soft robotics and stretch sensors [10]. For relaxation tests, samples are elongated up to several hundred percent and let them relax for a couple of hours. Under a logarithmic time axis as is shown in Fig. 6, for each Shore hardness, the actual stress remains a decreasing tendency over three hours of holding time, indicating that the equilibrium stress is not reached yet. A specimen of a higher Shore hardness yields a larger stress but a greater decrease of the overstress and a longer time to reach an equilibrium. If a pre-stretch is performed on specimens of any Shore hardness, the overstress diminishes largely, and therefore, the relaxation starts at a much smaller stress level and approaches the stress equilibrium quickly with a slight stress decrease, see Fig. 7. As we discussed in our previous Ecoflex 00-30 study summarised in [34], it is possible to assume that after a full relaxation, the overstress decreases significantly and a specimen reaches an equilibrium path that is time-independent. This equilibrium can also be reached at an earlier stage by a pre-stretch at a larger strain. The observations in the current section are consistent with this assumption.

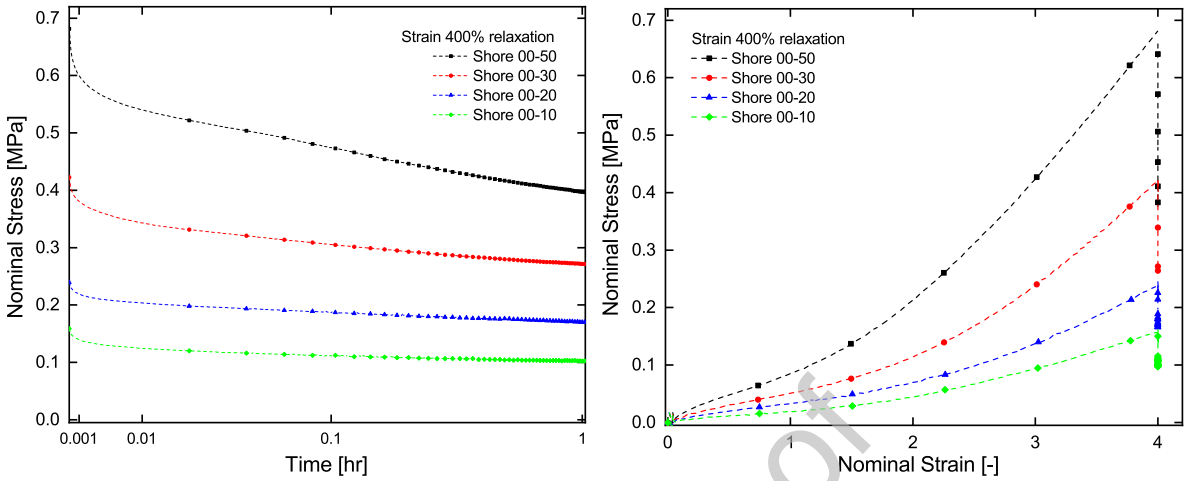

(a) (b)

Figure 6. Relaxation tests at 400% strain on different Shore hardnesses. (a) Stress evolution curves on logarithmic axis, (b) stress-strain curves.

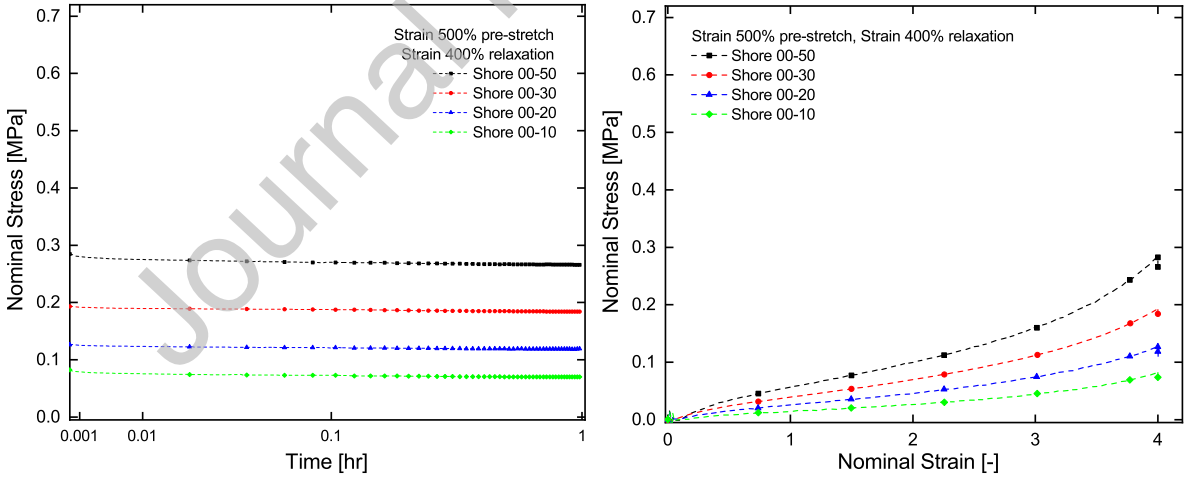

(a) (b)

Figure 7. Relaxation tests at 400% strain with a 500% strain pre-stretch on different Shore hardnesses. (a) Stress evolution curves on logarithmic axis, (b) stress-strain curves.

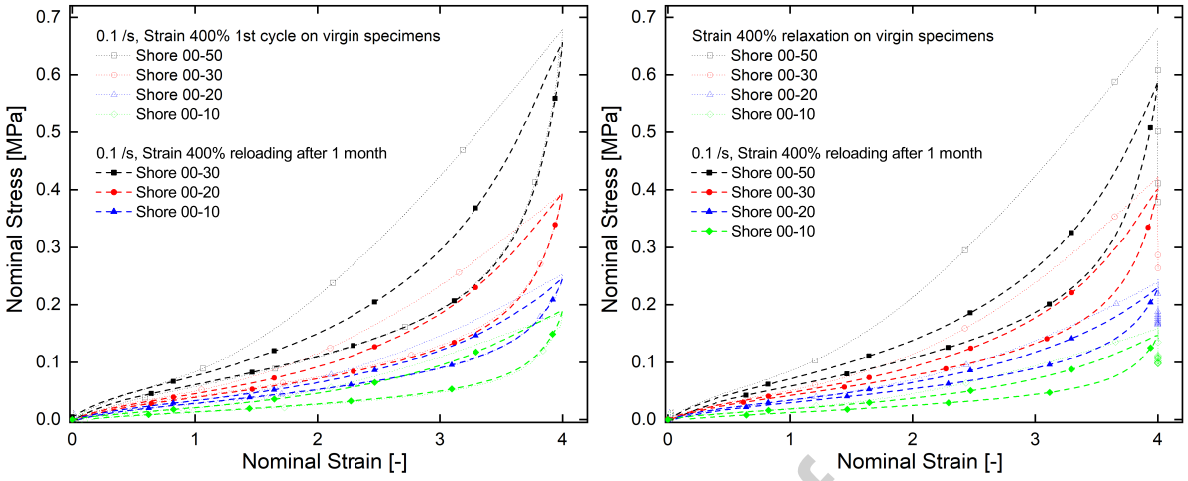

Figure 8. Stress recovery tests on different Shore hardnesses. (a) The first cycles on virgin specimens (shallow dotted curves) and the reloading cycles on the same specimens after one month rest time (dash curves) at 400% deformation, (b) the relaxation tests on virgin specimens (shallow dotted curves) and the reloading cycles on the same specimens after one month rest time (dash curves) at 400% deformation.

3.4. Stress recovery of Ecoflex

Many soft polymeric materials exhibit different kinds of stress recovery behaviour where some are significant while others are negligible [31, 35, 36, 37, 32]. However, in Ecoflex, the stress recovery is pronounced in all Shore hardnesses. Fig. 8(a) and Fig. 8(b) show that for all selected Shore hardnesses, after softening by a large deformation pre-treatment (dotted lines in Fig. 8(a)) or after relaxation by a long holding time pre-treatment, the stress reduction can recover with time (solid lines in Fig. 8(a) and Fig. 8(b), respectively). This means that the stress reduction in the overstress part is recoverable. Here, after one month, almost sixty percent overstress is recovered which might be further recovered if we can wait for a longer time, say one year. Note that although we present experimental results of the stress recovery, the modelling of this behaviour will be discussed in a further contribution.

3.5. Strain rate-and temperature-dependent behaviour

In this section, using Shore 00-30 as a representative, the strain rate and temperature dependences of Ecoflex are investigated, respectively. At first, load-unloading-reloading cyclic tests at different strain rates on virgin specimens are carried out. In this case, four different strain rates, i.e., 10^{-1} /s, 10^{-2} /s, 10^{-3} /s, 10^{-4} /s, are selected. A minor strain-rate dependence beyond 200% strain is observed from Fig. 9(a) where a higher strain rate results in a slightly larger stress. For example, with a four-decade span of time from 10^{-4} /s to 10^{-1} /s at 400% strain, the peak stress increases from 0.3 MPa to 0.4 MPa. This result is consistent with the time-dependent relaxation behaviour in the overstress part. In Fig. 9(b), we compare two reloading curves at 400% strain with two different strain rates after the removal of the overstress by a larger pre-stretch at 500%. Even though the strain rates in the graphs are five hundred times different, two curves are almost overlapped. This fact indicates that there is no strain rate dependence on this part. Hence, it can be considered as the

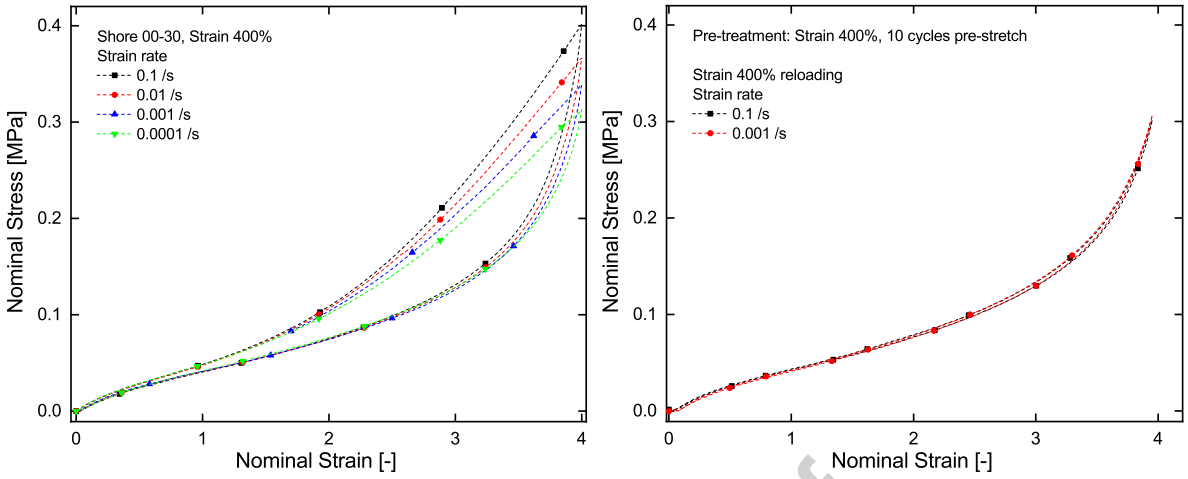

Figure 9. Strain rate-dependence tests on Shore 00-30. (a) Cyclic tests on virgin specimens at different strain rates, (b) reloading cyclic tests at different strain rates after a 500% pre-stretch.

equilibrium stress.

Several researchers illustrate that the mechanical properties of silicone polymers are sensitive to temperature variations [38, 39, 40]. Hence, a couple of cyclic tests with a strain of 400% under different temperatures are conducted which are presented in Fig. 10(a). It is clear from the figure that prior to 250% strain, the stress slightly increases as the temperature increases, which is very similar to other silicones as demonstrated by Rey et al. [38]. However, over the 250% strain, an opposite trend is observed, i.e., the stress magnitude decreases as the temperature increases. Moreover, the hysteresis decreases as the temperature increases. It might be case that the equilibrium part and overstress part have different dependences with respect to temperature. As explained by Li et al. [40], a positive temperature correlation may be caused by the entropy-related energy, while a negative temperature correlation is related to the enthalpy-related energy. On the one hand, prior to 250% strain, when the equilibrium stress becomes dominant, the total stress shows a positive correlation with the temperature increase. On the other hand, beyond 250% strain, when the overstress contribution becomes dominant, the total stress shows a negative correlation with the temperature increase.

Finally, we want to demonstrate the influences of temperature on equilibrium stresses as well as on the overstresses. For this, a pre-stretch with 500% strain at room temperature is performed first to all specimens. Fig. 10(b) illustrates test results at different temperatures at a strain of 400% after the removal of the overstress part. From a lower temperature to ambient and then to elevated temperature, the stress level of the equilibrium part undergoes a progressive increase. Since hysteresis is small before 200% strain, the equilibrium stress plays a dominant part in this strain range, where the total stress increases with the increasing temperature. Overall, it can be concluded that the polymer is somehow temperature-sensitive.

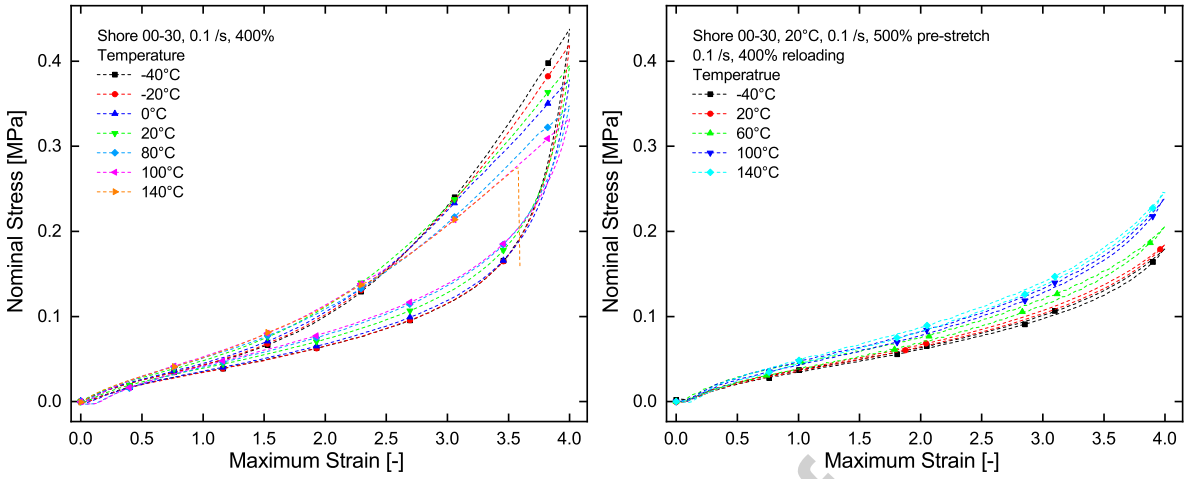

Figure 10. Temperature dependence tests on Shore 00-30. (a) Cyclic tests on virgin specimens at different temperatures, (b) reloading cyclic tests at different temperatures after a room temperature 500% pre-stretch.

4. Constitutive modelling of Ecoflex : Shore hardnesses and stress softening

Experimental results presented in the previous sections reveal that Ecoflex is almost insensitive to temperature and strain rate variations. However, the polymer shows significant stress softening and time-dependent stress recovery. Therefore, in the following section, a novel way to predict the mechanical responses of Ecoflex of different Shore hardnesses will be devised along with a constitutive model for capturing the stress softening. Modelling the time-dependent stress recovery phenomenon is deferred for future work. As we have already observed that Ecoflex with increasing Shore hardnesses behave very similarly to particle-filled polymers of increasing volume fractions. Therefore, an idea frequently used in modelling particle-filled polymers will be adopted [41, 42, 43]. Furthermore, in order to simulate the stress softening of different Shore hardnesses observed in Sec. 3.2, a so-called pseudo-elastic model originally proposed by Ogden and Roxburgh [44], Dorfmann and Ogden [45] is modified and adopted here.

4.1. Basic equations

For modelling polymeric materials, the deformation gradient $\mathbf{F} = \frac{\partial \boldsymbol{x}}{\partial \boldsymbol{X}}$ is used to represent large deformations, where $\boldsymbol{x}$ is the coordinate of a material point in the current configuration, while $\boldsymbol{X}$ is the same in the original configuration. The right Cauchy-Green strain tensor is defined as $\mathbf{C} = \mathbf{F}^{\mathrm{T}}\mathbf{F}$. The strain-energy function Ψ depends only on $\mathbf{F}$, then the first Piola stress tensor ($\mathbf{P}$) is expressed as

$$\mathbf{P} = \frac{\partial \Psi(\mathbf{F})}{\partial \mathbf{F}} = 2\mathbf{F}\frac{\partial \Psi(\mathbf{C})}{\partial \mathbf{C}}. \tag{1}$$

In general, the response of polymeric materials can be characterised by a strain energy function as

$$\Psi = \tilde{\Psi}(I_1, I_2, I_3). \tag{2}$$

In Eq. 2, the three strain invariants I_1, I_2, I_3 of $\mathbf{C}$ are defined as $I_1 = \lambda_1^2+\lambda_2^2+\lambda_3^2$; $I_2 = \lambda_1^2\lambda_2^2+\lambda_2^2\lambda_3^2+\lambda_1^2\lambda_3^2$; $I_3 = \lambda_1^2\lambda_2^2\lambda_3^2$, where $\lambda_1^2, \lambda_2^2, \lambda_3^2$ are the eigenvalues of the deformation tensor $\mathbf{C}$. The square roots of

the eigenvalues λ_1, λ_2 and λ_3 are principle stretches, denoting deformations in the x, y and z directions, respectively. Since polymeric materials are generally considered as incompressible materials, i.e., $I_3 = 1$, with Eq. 2, the first Piola stress tensor can be derived (after imposing the incompressibility constraint) as

$$\mathbf{P} = -p\mathbf{F}^{-\mathrm{T}} + 2\left[\frac{\partial \Psi}{\partial I_1} + I_1\frac{\partial \Psi}{\partial I_2}\right]\mathbf{F} - 2\frac{\partial \Psi}{\partial I_2}\mathbf{F}\cdot\mathbf{C}, \tag{3}$$

where, p is a scalar Lagrange multiplier which will be determined by appropriate boundary conditions, and $\mathbf{F}^{-1}$ is the inverse of the deformation gradient tensor $\mathbf{F}$. Now, specific energy functions need to be introduced. As is discussed in the literature [46, 47, 20, 48], there are two modelling approaches for polymers, i) micro-mechanically motivated models and ii) phenomenological-motivated models. Among them the Neo-Hookean model has both the micro-mechanical and phenomenological explanations [49, 48]. In this work, two widely-used first invariant-based energy functions, e.g., Neo-Hooke (NH) and Yeoh (Y) are adopted,

$$\Psi_{\mathrm{NH}} = \frac{\mu}{2}\left[I_1 - 3\right], \quad \Psi_{\mathrm{Y}} = c_1\left[I_1 - 3\right] + c_2\left[I_1 - 3\right]^2 + c_3\left[I_1 - 3\right]^3, \tag{4}$$

where, μ, c_1, c_2, c_3 are material parameters of respective models that need to be identified from experimental data, see Steinmann et al. [50]. For these first-invariant-based models, the expression in Eq. 3 can be simplified as

$$\mathbf{P} = -p\mathbf{F}^{-\mathrm{T}} + 2\frac{\partial \Psi}{\partial I_1}\mathbf{F}. \tag{5}$$

All conducted experiments in our study mentioned above fulfil usual dimensions of a uniaxial deformation, i.e., $\lambda_1 = \lambda, \lambda_2 = \lambda_3 = 1/\sqrt{\lambda}$ $(\lambda_1^2\lambda_2^2\lambda_3^2 = 1)$ and $I_1 = 2\lambda^{-1} + \lambda^2$ as the deformation gradient reads $\mathbf{F} = \mathrm{diag}\left\{\lambda_1, \lambda_2, \lambda_3\right\} = \mathrm{diag}\left\{\lambda, \lambda^{-\frac{1}{2}}, \lambda^{-\frac{1}{2}}\right\}$. Substituting Eq. 4 into Eq. 5 and combining the uniaxial deformation condition along with the incompressible condition, the nominal stress expressions of the two models can be given by

$$P_{\mathrm{NH}} = \mu\left[\lambda - \lambda^{-2}\right], \quad P_{\mathrm{Y}} = \left[2c_1 + 4c_2\left[I_1 - 3\right] + 6c_3\left[I_1 - 3\right]^2\right]\left[\lambda - \lambda^{-2}\right]. \tag{6}$$

For detailed derivations of Eq. 6, readers may consult the works of Steinmann et al. [50], Hossain et al. [46, 47, 20], Liao et al. [22].

4.2. Modelling stress softening

Stress softening, or so-called Mullins effect [51] is a very common phenomenon of polymeric materials. This behaviour is significantly observed in Ecoflex of all Shore hardnesses as discussed in Sec. 3.2. Constitutive approaches to predict such a phenomenon are mainly classified into two types; phenomenological models, cf. [44, 45, 52], and micro-mechanical models, cf. [42, 53]. In this study, a pseudo-elastic phenomenological model for the stress softening proposed by Ogden and co-workers [44, 45] is mainly adopted. Note that in our case, the stress softening only happens in the overstress part while the equilibrium part is not dependent on the strain history.

For a certain energy function Ψ, if the stress softening is considered, then, in addition to deformation variable, an additional internal variable η is added to the energy function, i.e., $\Psi = \Psi(\mathbf{F}, \eta) = \Psi(I_1, I_2, \eta)$.

According to Ogden and co-workers [44, 45], the additional internal variable has to satisfy

$$\frac{\partial \Psi}{\partial \eta}(I_1, I_2, \eta) = 0. \tag{7}$$

From Eq. 7, under the incompressible condition, i.e., $I_3 = 1$, the Piola stress tensor yields the same form as Eq. 3. If η denotes the ratio of energies before and after softening and if the energy function is only dependent on I_1, it can then be specialized as

$$\Psi\left(I_1, \eta\right) = \eta \Psi_0\left(I_1\right) + \phi(\eta), \tag{8}$$

where, Ψ_0 denotes the energy function of a virgin specimen without any stress softening (on the primary loading path), e.g., Eq. 4 and ϕ refers to as the damage energy function which denotes the energy dissipation required to cause any softening. Now Eq. 7 has a clear physical connotation: the total energy Ψ (the summation of the residual energy $\eta\Psi_0$ and the dissipation energy ϕ) at a certain deformation is conservative and is not influenced by η. From Eq. 8 and Eq. 5, the nominal stress is deducted as

$$P = \eta P_0, \tag{9}$$

where, P_0 is the nominal stress in the primary loading path, such in Eq. 6 and then Eq. 7 becomes

$$\phi'(\eta) = -\Psi_0\left(I_1\right), \tag{10}$$

which implicitly determines η. When $\eta = 1$, no softening happens, and therefore no dissipation is caused by the softening. This requires that in Eq. 8,

$$\phi(1) = 0, \tag{11}$$

and in Eq. 10,

$$-\phi'(1) = \Psi_0\left(I_{1,\max}\right) = \Psi_{\max}, \tag{12}$$

where, $I_{1,\max}$ denotes the maximum first invariant in the deformation history, and $\Psi_{\max}$ is defined as the present maximum energy on the primary loading path where an unloading initiates. Then $\phi(\eta)$ is defined based on the constraints of Eq. 11 and Eq. 12. Here, we select a hyperbolic function which is a modified version initially proposed by Dorfmann and Ogden [45],

$$-\phi'(\eta) = -\mu_0 m \tanh^{-1}\left(r\left[1-\eta\right]\right) + \Psi_{\max}, \tag{13}$$

where, m, r and q are material parameters that need to be determined, and μ_0 is a stiffness parameter taken as 1 MPa. After a simple algebraic calculation, an expression for the internal variable is obtained as

$$\eta = 1 - \frac{1}{r}\tanh\left(\frac{\Psi_{\max} - \Psi_0(I_1)}{\mu_0 m}\right). \tag{14}$$

For a detailed deduction of the equations, readers may refer to [44, 45, 54].

4.3. Amplification factor for Shore variation of Ecoflex

As we have observed and discussed in Sec. 3.2 that the stress enhancements and the dissipations due to the cyclic loading of Ecoflex of different Shore hardnesses are very similar to particle-filled polymers. For the

modelling of Shore-dependent Ecoflex, an approach mainly used in modelling particle-filled polymers will be revisited here. In order to account for the stress enhancements by hard filler particles, the first approach is the amplified stretch Λ, which in the case of a uniaxial loading, is related to the actual axial stretch λ by $\Lambda = 1 + X[\lambda - 1]$, where, X is a stretch amplification factor that depends on the volume fraction of fillers, v_f. According to the Mullins-Tobin assumption [55], in order to obtain complete stress-strain expressions to capture the effects of rigid filler particles, the actual stretch λ needs to be replaced by the amplified stretch Λ in rubber-like material models such as in Eq. 6. Alshammari et al. [43] very recently incorporated the idea for the modelling of graphite filled PET micro-composites. However, this approach is simply an amplification of the uniaxial stretch λ. Hence, Bergstroem and Boyce [4] further developed this approach into a three-dimensional format by amplifying the first invariant I_1 instead of stretch λ. In this contribution, we adopt an idea which is similar to the one proposed by Bergstroem and Boyce [4] for the modelling of particle-filled polymers as

$$I_{1,h} = X[I_1 - 3] + 3 \tag{15}$$

where, $I_{1,h}$ is the amplified first invariant to incorporate Shore influences. This approach can be applied to any I_1-based model such as Neo-Hooke, Yeoh, Arruda-Boyce, Gent, etc. According to Guth model [41], the application factor X can be defined as

$$X = 1 + 0.67gv_f + 1.62[gv_f]^2, \tag{16}$$

where, v_f is the weight fraction of fillers and g is a factor describing the asymmetric nature of the aggregated clusters. In this study, this idea is generalised to the case of Ecoflex with Shore variations. Here, a normalized variable of the Shore hardness s is defined as

$$s = \frac{H}{H_0} - 1, \tag{17}$$

where, H is the last two digits of an actual Shore hardness, and H_0 is the same of the reference Shore hardness. For our case, the reference material is Shore 00-10, where $H_0 = 10$. We consider that with a different s, the micro-mechanical behaviour has a similar variation as changing fillers, and therefore the amplification factor can be considered analogous to Eq. 16 as

$$X = 1 + g_1 s + g_2 s^2, \tag{18}$$

where, g_1 and g_2 are material parameters.

4.4. Combination of Shore variation and stress softening model

As we discussed in the previous sections, the total stress of Ecoflex consists of an equilibrium part and an overstress part. Furthermore, it is observed that each portion of stress has different dependences. On this ground, the model will be developed for each stress portion separately. Note that in this work, our focus is to characterise the mechanical response dependent on Shore hardness variations. Modelling of the time-dependent stress recovery behaviour will be dealt with in a forthcoming contribution. From the experimental results, it is observed that the equilibrium stress exhibits an overall decreasing slope, for which, a Neo-Hookean equation (Eq. 4) is an appropriate choice to model the tendency. As the amplified first strain invariant is employed, the energy function for the equilibrium part thus reads

$$\Psi^{\text{eq}}(I^{\text{eq}}_{1,h}) = \frac{\mu}{2}\left[I^{\text{eq}}_{1,h} - 3\right], \quad I^{\text{eq}}_{1,h} = X^{\text{eq}}[I_1 - 3] + 3, \quad X^{\text{eq}} = 1 + g^{\text{eq}}_1 s + g^{\text{eq}}_2 s^2, \tag{19}$$

where, $I^{\text{eq}}_{1,h}$, X^{eq}, and g^{eq}_i $(i = 1, 2)$ are the amplified first strain invariant, amplification factor and material parameters, respectively, for the equilibrium part. Following the same procedure as in Sec. 4.1, substituting the energy function Eq. 4 into Eq. 5 and combining the uniaxial deformation and the incompressibility conditions, the nominal stress is obtained as

$$P^{\text{eq}} = X^{\text{eq}}\mu\left[\lambda - \lambda^{-2}\right]. \tag{20}$$

For the overstress part, a Yeoh energy function (Eq. 4) is adopted in light of the upward trend of the total stress. After incorporating the amplified first strain invariant $I_{1,h}$, the energy function reads

$$\Psi^{\text{ov}}_0(I^{\text{ov}}_{1,h}) = c_1\left[I^{\text{ov}}_{1,h} - 3\right] + c_2\left[I^{\text{ov}}_{1,h} - 3\right]^2 + c_3\left[I^{\text{ov}}_{1,h} - 3\right]^3, \tag{21a}$$

$$I^{\text{ov}}_{1,h} = X^{\text{ov}}[I_1 - 3] + 3, \quad X^{\text{ov}} = 1 + g^{\text{ov}}_1 s + g^{\text{ov}}_2 s^2. \tag{21b}$$

where $I^{\text{ov}}_{1,h}$, X^{ov}, and g^{ov}_i $(i = 1, 2)$ are the amplified first strain invariant, amplification factor and undetermined parameters, respectively, for the overstress part. Note that we have used different amplification factors, X^{eq} and X^{ov}, for the responses of each part, under the consideration that their dependences on the Shore hardness may be different. The subscript 0 again denotes that the energy function Ψ^{ov}_0 describes the material response on the primary loading path. Following the similar approach as in the equilibrium part, substituting the energy function Eq. 21 into Eq. 5 and using the incompressible condition, the uniaxial nominal stress for the primary path is obtained as

$$P^{\text{ov}}_0 = X^{\text{ov}}\left[2c_1 + 4c_2\left[I^{\text{ov}}_{1,h} - 3\right] + 6c_3\left[I^{\text{ov}}_{1,h} - 3\right]^2\right]\left[\lambda - \lambda^{-2}\right]. \tag{22}$$

Note that the softening takes place in the overstress part only. Based on the equation in Sec. 4.2, the amplified energy function in Eq. 4 is used in Eq. 9 and Eq. 14. Then the overstress is given by

$$P^{\text{ov}} = \eta P^{\text{ov}}_0. \tag{23}$$

Finally, a complete set of constitutive equations in combination with the equilibrium and the overstress parts are given:

$$P = P^{\text{eq}} + P^{\text{ov}} = \left[X^{\text{eq}}\mu + \eta X^{\text{ov}}\left[2c_1 + 4c_2\left[I^{\text{ov}}_{1,h} - 3\right] + 6c_3\left[I^{\text{ov}}_{1,h} - 3\right]^2\right]\right]\left[\lambda - \lambda^{-2}\right], \tag{24a}$$

$$X^{\text{eq}} = 1 + g^{\text{eq}}_1 s + g^{\text{eq}}_2 s^2, \quad X^{\text{ov}} = 1 + g^{\text{ov}}_1 s + g^{\text{ov}}_2 s^2, \quad I^{\text{ov}}_{1,h} = X^{\text{ov}}[I_1 - 3] + 3, \tag{24b}$$

$$\eta = 1 - \frac{1}{r}\tanh\left(\frac{\Psi^{\text{ov}}(I^{\text{ov}}_{1,h,\max}) - \Psi^{\text{ov}}(I^{\text{ov}}_{1,h})}{\mu_0 m}\right), \tag{24c}$$

$$\Psi^{\text{ov}} = c_1[I^{\text{ov}}_{1,h} - 3] + c_2[I^{\text{ov}}_{1,h} - 3]^2 + c_3[I^{\text{ov}}_{1,h} - 3]^3. \tag{24d}$$

5. Parameter identification and model validation

In this study, for the parameter identification, a least square curve-fitting approach (`lsqcurvefit`) built-in within the commercial mathematical software MATLAB is adopted. Under such an approach, the difference between experimental data and the constitutive equations is minimized by optimizing relevant material parameters appearing in the models.

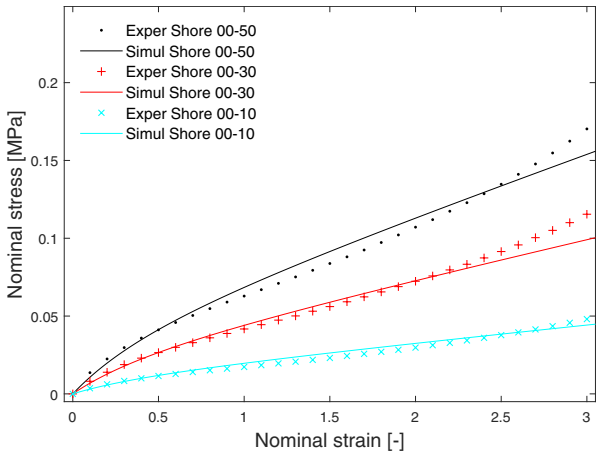

Figure 11. Parameters' identification from the equilibrium stress data: Equilibrium paths of Shore hardnesses 00-50, 00-30, and 00-10 after a 500% pre-stretch are used.

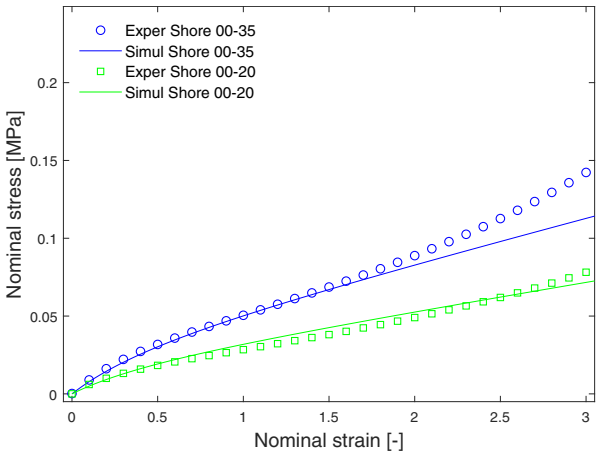

Figure 12. Equilibrium parameters validation: Equilibrium paths of Shore hardnesses 00-35 and 00-20 after a 500% pre-stretch are used.

5.1. *Equilibrium part*

At first, the identification of parameters appearing in the equilibrium stress of different Shore hardnesses is carried out. As is mentioned in [34], the overstress part can be removed significantly by a pre-stretch at a larger strain. Therefore, we adopt the reloading curves after a 500% pre-stretch of each Shore hardness specimen for the equilibrium path fitting which is the stress-strain data from Fig. 7(b). Even so, at strain level close to that of the pre-stretch, the overstress is not entirely removed. Therefore, the equilibrium stress is overestimated. Accordingly, we only adopt data before 300% deformation for parameters calibration.

In the parameter identification, the data of Shore hardnesses 00-50, 00-30, and 00-10 are adopted. The fitting results are shown in Fig. 11, where the dotted lines are experimental data and the solid lines are simulation curves. Once model parameters are identified, they need to be validated with experimental data sets which are not used in the parameter identification. Experimental data of Shore hardnesses 00-35 and 00-20 are used for the validation of the model, see Fig. 12, where the dotted lines are experimental data and the solid lines are validation curves. The model prediction nicely coincides with the experimental data. For identified material parameters in the equilibrium part, see Tab. 2.

5.2. *Overstress part*

Once the parameter set appearing in the equilibrium part of the model is identified, the next step is to calibrate the overstress parameters. For this, the experiment data of the total stress of the primary loading path obtained from virgin specimens on different Shore hardnesses are adopted from Fig. 4(a). In combination with the equilibrium part with identified parameters, the overstress parameters can be identified from the total stress data. Similarly, Shore hardnesses 00-50, 00-30, and 00-10 are used for the calibration, see Fig. 13, where the dotted lines are experimental data while the solid lines are simulation curves. Afterwards, Shore hardnesses 00-35, 00-20 are used for the model validation, see Fig. 14, where the dotted lines are experimental data and the solid lines are validation curves. Note that upon the primary loading, the stress softening is not activated in the energy function since $\eta = 1$. Hence, the parameters of the energy function in the overstress part are decoupled from the stress softening ones, and can be identified independently in

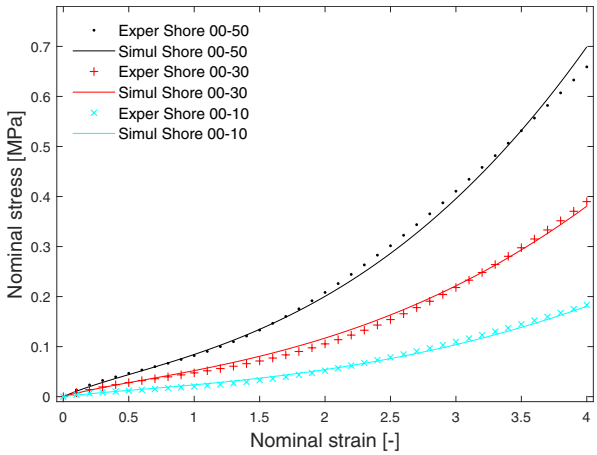

Figure 13. Parameters' identification from the total stress data: Primary loading paths of Shore hardnesses 00-50, 00-30, and 00-10 are used.

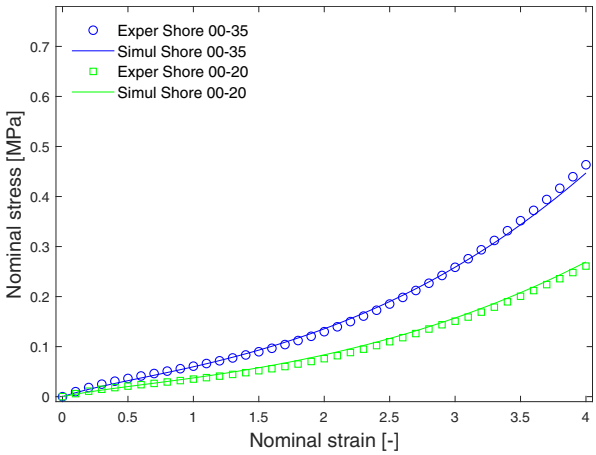

Figure 14. Parameters' validation using the total stress data: Primary loading paths of Shore hardnesses 00-35 and 00-20 are used.

Table 2: Identification of complete parameters' set : two parameters for the equilibrium section, four parameters for the overstress section, and two for the stress softening

μ [MPa]	g_1^{eq} [1]	c_1 [MPa]	c_2 [MPa]	g_1^{ov} [1]	g_2^{ov} [1]	m [1]	r [1]
1.123e-02	6.202e-01	2.220e-14	2.810e-04	1.788e-01	1.851e-02	4.673e-02	1.224e+00

the following section.

5.3. Stress softening

All parameters related to the equilibrium and the overstress parts are identified and validated in the previous two sections. Now, the parameters of the pseudo-elastic model for the stress softening are to be identified. Since we focus on the stress softening and the viscoelasticity is a very insignificant phenomenon here, the minimal hysteresis effect is ignored in the modelling. The second reloading data from Fig. 4(b) at strain 400% of different Shore hardnesses is used for the identification of softening parameters. In this case, the data for Shore 00-50, 00-30, and 00-10 are used for the model calibration, as is shown in Fig. 15, while data of Shore hardnesses 00-35 and 00-20 are used for the validation, as is shown in Fig. 16.

A further validation of our proposed model is made by few multi-cycle tests with increasing strain levels on different Shore hardnesses. The results are illustrated in Fig. 17. It is shown that the predicted results show very good agreement with the experimental data. The complete set of the identified parameters are shown in Tab. 2. It is found that c_3 and g_2^{eq} are close to zero, and r is close to one, implying that they have little influences on the constitutive equations. Furthermore, $r = 1$ also means that when the deformation is large enough, we have $\eta = 0$, which denotes that the overstress is removed totally. Therefore, the complete constitutive equations for the Ecoflex silicone rubber with different Shore hardnesses with combination of the equilibrium part and the overstress part are given with only eight material parameters.

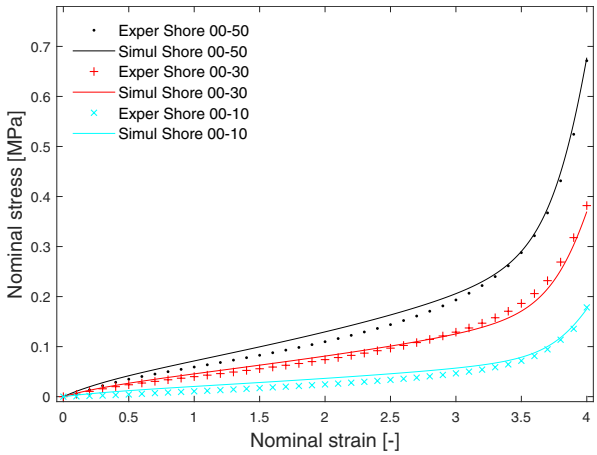

Figure 15. Parameters' identification of the pseudo-elastic model for stress softening: First reloading paths of Shore hardnesses 00-50, 00-30, and 00-10 are used.

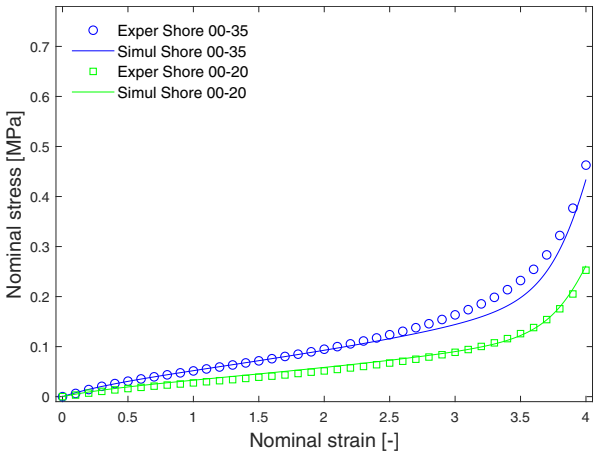

Figure 16. Parameters' validation of the pseudo-elastic model for stress softening: First reloading paths of Shore hardnesses 00-35 and 00-20 are used.

6. Conclusions

In this study, at first, we carry out a systematic and comprehensive experimental study on Ecoflex of five different Shore hardnesses. These tests include loading and unloading cyclic tests with the same strain level and tests with increasing strain levels, relaxation tests with and without a larger pre-stretch, and stretchability tests on different Shore hardnesses. Stiffness, hysteresis, relaxation time, equilibrium stress, the amount of stress reduction after relaxation and softening, etc., increase with an increasing Shore hardness. Based on the experimental results, the stress-strain response can be decomposed into equilibrium and overstress parts, and the forms of dependence are different on two separate parts.

Analysing the experimental findings, we propose a novel strategy to model the Shore influence on the stress-strain responses of Ecoflex. To describe the decreasing slope trend of the equilibrium part, we adopt a modified Neo-Hookean model, where the stiffness enhancement is related to a function of the Shore hardness variable. For the overstress part, a Yeoh model is adopted to embody the increasing slope of the data. Both energy functions incorporate the concept of amplified strain invariant, where an amplifying factor is used to describe the dependence of the Shore hardness. Afterwards, a pseudo-elastic model is adopted for predicting the stress softening behaviour. The simulation results based on our newly developed model reproduce the experimental data with a good agreement on the equilibrium path, overstress on the primary loading path and the subsequent unloading and reloading paths. The comprehensive thermo-viscoelastic study sets a guideline for conducting experimental procedures to soft polymers appearing with several Shore hardnesses. Furthermore, the novel Shore-based modelling strategy at finite strain presented herein can easily be applied to other polymers which have various Shore hardnesses as of Ecoflex.

Declaration of Competing interests

The authors declare that they have no known competing financial interests or personal relationships that could have appeared to influence the work reported in this paper.

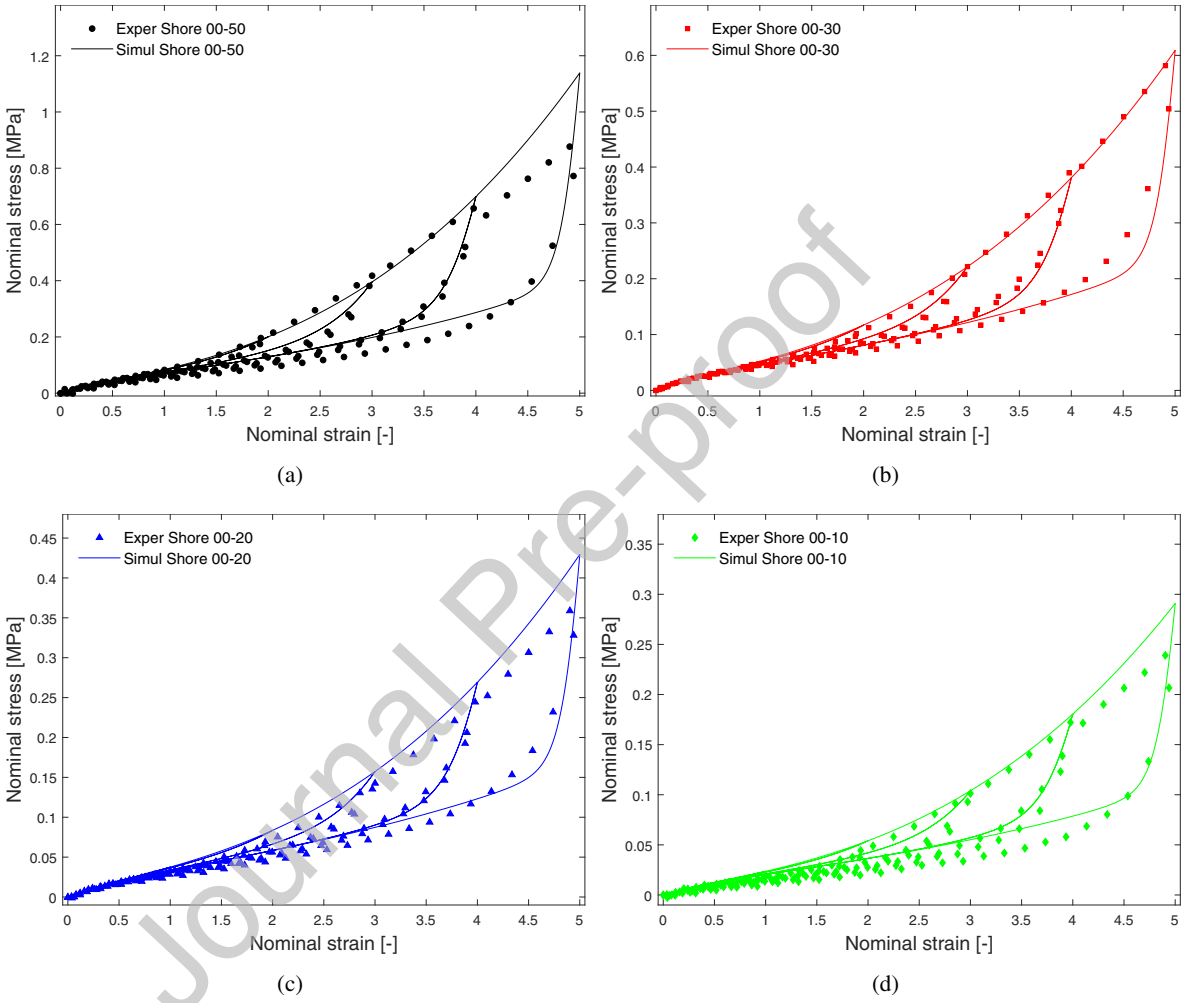

Figure 17. Model validation by multi-cycle tests with increasing strain levels. (a) Shore hardness 00-50, (b) Shore hardness 00-30, (c) Shore hardness 00-20, (d) Shore hardness 00-10.

Acknowledgements

This work is partially supported by the National Science Fund for Distinguished Young Scholars (Nos.11925203) and the National Natural Science Foundation of China (Nos. 1672110). The work is also benefited from the Fundamental Research Funds for the Central Universities, SCUT (2018PY21). The first two authors would like to extend their sincere appreciation to Zienkiewicz Centre for Computational Engineering (ZCCE), Swansea University, UK for supporting the work. The support facilitates an exchange visit of the first author to ZCCE.

References

[1] L. Bernardi, R. Hopf, A. Ferrari, A. Ehret, E. Mazza, On the large strain deformation behavior of silicone-based elastomers for biomedical applications, Polymer Testing 58 (2017) 189–198. doi:10.1016/j.polymertesting.2016.12.029.

[2] L. Bernardi, R. Hopf, D. Sibilio, A. Ferrari, A. Ehret, E. Mazza, On the cyclic deformation behavior, fracture properties and cytotoxicity of silicone-based elastomers for biomedical applications, Polymer Testing 60 (2017) 117–123. doi:10.1016/j.polymertesting.2017.03.018.

[3] O. A. Shergold, N. A. Fleck, D. Radford, The uniaxial stress versus strain response of pig skin and silicone rubber at low and high strain rates, International Journal of Impact Engineering 32 (9) (2006) 1384–1402. doi:10.1016/j.ijimpeng.2004.11.010.

[4] J. S. Bergstroem, Large strain time-dependent behavior of elastomeric materials, Phd dissertation, Massachusetts Institute of Technology, USA (1999).

[5] H. Hoeksema, M. D. Vos, J. Verbelen, A. Pirayesh, S. Monstrey, Scar management by means of occlusion and hydration: A comparative study of silicones versus a hydrating gel-cream, Burns 39 (7) (2013) 1437–1448. doi:10.1016/j.burns.2013.03.025.

[6] J. C. Case, E. L. White, R. K. Kramer, Soft material characterization for robotic applications, Soft Robotics 2 (2) (2015) 80–87. doi:10.1089/soro.2015.0002.

[7] S. Zakaria, L. Yu, G. Kofod, A. L. Skov, The influence of static pre-stretching on the mechanical ageing of filled silicone rubbers for dielectric elastomer applications, Materials Today Communications 4 (2015) 204–213. doi:10.1016/j.mtcomm.2015.08.002.

[8] M. Mehnert, M. Hossain, P. Steinmann, Numerical modeling of thermo-electro-viscoelasticity with field-dependent material parameters, International Journal of Non-Linear Mechanics 106 (2018) 13–24. doi:10.1016/j.ijnonlinmec.2018.08.016.

[9] M. Amjadi, Y. J. Yoon, I. Park, Ultra-stretchable and skin-mountable strain sensors using carbon nanotubes–ecoflex nanocomposites, Nanotechnology 26 (37) (2015) 375501. doi:10.1088/0957-4484/26/37/375501.

[10] Sibo Cheng and Baohong Chen and Yuan Zhou and Minglong Xu and Zhigang Suo, Soft sensor for full dentition dynamic bite force, Extreme Mechanics Letters 34 (2020) 100592. doi:10.1016/j.eml.2019.100592.

[11] Huy Mai and Rahim Mutlu and Charbel Tawk and Gursel Alici and Vitor Sencadas, Ultra-stretchable MWCNT–Ecoflex piezoresistive sensors for human motion detection applications, Composites Science and Technology 173 (2019) 118–124. doi:10.1016/j.compscitech.2019.02.001.

[12] Seong Jun Kim and Shuvra Mondal and Bok Ki Min and Choon-Gi Choi, Highly Sensitive and Flexible Strain–Pressure Sensors with Cracked Paddy-Shaped MoS2/Graphene Foam/Ecoflex Hybrid Nanostructures, ACS Applied Materials & Interfaces 10 (42) (2018) 36377–36384. doi:10.1021/acsami.8b11233.

[13] Jin-Woong Lee and Jiyong Chung and Min-Young Cho and Suman Timilsina and Keemin Sohn and Ji Sik Kim and Kee-Sun Sohn, Deep-Learning Technique To Convert a Crude Piezoresistive Carbon Nanotube-Ecoflex Composite Sheet into a Smart, Portable, Disposable, and Extremely Flexible Keypad, ACS Applied Materials & Interfaces 10 (24) (2018) 20862–20868. doi:10.1021/acsami.8b04914.

[14] Yuting Jiang and Yang Wang and Yogendra Kumar Mishra and Rainer Adelung and Ya Yang, Stretchable CNTs-Ecoflex Composite as Variable-Transmittance Skin for Ultrasensitive Strain Sensing, Advanced Materials Technologies 3 (12) (2018) 1800248. doi:10.1002/admt.201800248.

[15] I. Collins, M. Hossain, I. Masters, A review of flexible structures for wave energy converters, European Wave Tidal and Energy Conference Series 13 (1) (2019) 1–10.

[16] C.L.Zhang, Z.H.Lai, X.X.Rao, J.W.Zhang, D.Yurchenkoc, Energy harvesting from a novel contact-type dielectric elastomer generator, Energy Conversion and Management 205 (1) (2020) 112351. doi:10.1016/j.enconman.2019.112351.

[17] L. Guo, Y. Lv, Z. Deng, Y. Wang, X. Zan, Tension testing of silicone rubber at high strain rates, Polymer Testing 50 (2016) 270–275. doi:10.1016/j.polymertesting.2016.01.021.

[18] J. L. Sparks, N. A. Vavalle, K. E. Kasting, B. Long, M. L. Tanaka, P. A. Sanger, K. Schnell, T. A. Conner-Kerr, Use of silicone materials to simulate tissue biomechanics as related to deep tissue injury, Advances in Skin & Wound Care 28 (2) (2015) 59–68. doi:10.1097/01.asw.0000460127.47415.6e.

[19] D. Steck, J. Qu, S. B. Kordmahale, D. Tscharnuter, A. Muliana, J. Kameoka, Mechanical responses of ecoflex silicone rubber: Compressible and incompressible behaviors, Journal of Applied Polymer Science 136 (5) (2018) 47025. doi:10.1002/app.47025.

[20] M. Hossain, D. K. Vu, P. Steinmann, Experimental study and numerical modelling of VHB 4910 polymer, Computational Materials Science 59 (2012) 65–74. doi:10.1016/j.commatsci.2012.02.027.

[21] M. Johlitz, H. Steeb, S. Diebels, A. Chatzouridou, J. Batal, W. Possart, Experimental and theoretical investigation of nonlinear viscoelastic polyurethane systems, Journal of Materials Science 42 (23) (2007) 9894–9904. doi:10.1007/s10853-006-1479-4.

[22] Z. Liao, M. Hossain, X. Yao, M. Mehnert, P. Steinmann, On thermo-viscoelastic experimental characterization and numerical modelling of VHB polymer, International Journal of Non-Linear Mechanics 118 (2020) 103263. doi:10.1016/j.ijnonlinmec.2019.103263.

[23] M. Wissler, E. Mazza, Mechanical behavior of an acrylic elastomer used in dielectric elastomer actuators, Sensors and Actuators A: Physical 134 (2) (2007) 494–504. doi:10.1016/j.sna.2006.05.024.

[24] R. Sahu, K. Patra, J. Szpunar, Experimental study and numerical modelling of creep and stress relaxation of dielectric elastomers, Strain 51 (1) (2014) 43–54. doi:10.1111/str.12117.

[25] X. Zhang, H. Hao, Y. Shi, J. Cui, The mechanical properties of polyvinyl butyral (PVB) at high strain rates, Construction and Building Materials 93 (2015) 404–415. doi:10.1016/j.conbuildmat.2015.04.057.

[26] Z. Liao, X. Yao, L. Zhang, M. Hossain, J. Wang, S. Zang, Temperature and strain rate dependent large tensile deformation and tensile failure behavior of transparent polyurethane at intermediate strain rates, International Journal of Impact Engineering 129 (2019) 152–167. doi:10.1016/j.ijimpeng.2019.03.005.

[27] J. Bergstroem, M. Boyce, Large strain time-dependent behavior of filled elastomers, Mechanics of Materials 32 (11) (2000) 627–644. doi:10.1016/s0167-6636(00)00028-4.

[28] S. Wang, S. A. Chester, Experimental characterization and continuum modeling of inelasticity in filled rubber-like materials, International Journal of Solids and Structures 136-137 (2018) 125–136. doi:10.1016/j.ijsolstr.2017.12.010.

[29] L. Mullins, Effect of stretching on the properties of rubber, Rubber Chemistry and Technology 21 (2) (1948) 281–300. doi:10.5254/1.3546914.

[30] J. A. C. Harwood, A. R. Payne, Stress softening in natural rubber vulcanizates. part IV. unfilled vulcanizates, Journal of Applied Polymer Science 10 (8) (1966) 1203–1211. doi:10.1002/app.1966.070100811.

[31] J. Diani, B. Fayolle, P. Gilormini, A review on the mullins effect, European Polymer Journal 45 (3) (2009) 601–612. doi:10.1016/j.eurpolymj.2008.11.017.

[32] D. E. Hanson, M. Hawley, R. Houlton, K. Chitanvis, P. Rae, E. B. Orler, D. A. Wrobleski, Stress softening experiments in silica-filled polydimethylsiloxane provide insight into a mechanism for the mullins effect, Polymer 46 (24) (2005) 10989–10995. doi:10.1016/j.polymer.2005.09.039.

[33] G. Machado, G. Chagnon, D. Favier, Analysis of the isotropic models of the mullins effect based on filled silicone rubber experimental results, Mechanics of Materials 42 (9) (2010) 841–851. doi:10.1016/j.mechmat.2010.07.001.

[34] Z. Liao, M. Hossain, X. Yao, R. Navaratne, G. Chagnon, A comprehensive thermo-viscoelastic experimental investigation of ecoflex polymer, Polymer Testing 2019 (In Review) 1–20.

[35] J. Plagge, M. Klueppel, Mullins effect revisited: Relaxation, recovery and high-strain damage, Materials Today Communications 20 (2019) 100588. doi:10.1016/j.mtcomm.2019.100588.

[36] S. Wang, S. A. Chester, Modeling thermal recovery of the mullins effect, Mechanics of Materials 126 (2018) 88–98. doi:10.1016/j.mechmat.2018.08.002.

[37] L. Yan, D. A. Dillard, R. L. West, L. D. Lower, G. V. Gordon, Mullins effect recovery of a nanoparticle-filled polymer, Journal of Polymer Science Part B: Polymer Physics 48 (21) (2010) 2207–2214. doi:10.1002/polb.22102.

[38] T. Rey, G. Chagnon, J.-B. L. Cam, D. Favier, Influence of the temperature on the mechanical behaviour of filled and unfilled silicone rubbers, Polymer Testing 32 (3) (2013) 492–501. doi:10.1016/j.polymertesting.2013.01.008.

[39] L. Guo, Y. Wang, HIGH-RATE TENSILE BEHAVIOR OF SILICONE RUBBER AT VARIOUS TEMPERATURES, Rubber Chemistry and Technology (In-Press). doi:10.5254/rct.19.81562.

[40] X. Li, T. Bai, Z. Li, L. Liu, Influence of the temperature on the hyper-elastic mechanical behavior of carbon black filled natural rubbers, Mechanics of Materials 95 (2016) 136–145. doi:10.1016/j.mechmat.2016.01.010.

[41] E. Guth, Theory of filler reinforcement, Journal of Applied Physics 16 (1) (1945) 20–25. doi:10.1063/1.1707495.

[42] J. S. Bergstroem, M. C. Boyce, Constitutive modeling of the large strain time-dependent behavior of elastomers, Journal of the Mechanics and Physics of Solids 46 (5) (1998) 931–954. doi:10.1016/S0022-5096(97)00075-6.

[43] B. A. Alshammari, F. S. Al-Mubaddel, M. R. Karim, M. Hossain, A. S. Al-Mutairi, A. N. Wilkinson, Addition of graphite filler to enhance electrical, morphological, thermal, and mechanical properties in poly (ethylene terephthalate): Experimental characterization and material modeling, Polymers 11 (9) (2019) 1411. doi:10.3390/polym11091411.

[44] R. W. Ogden, D. G. Roxburgh, A pseudo–elastic model for the mullins effect in filled rubber, Proceedings of the Royal Society of London. Series A: Mathematical, Physical and Engineering Sciences 455 (1988) (1999) 2861–2877. doi:10.1098/rspa.1999.0431.

[45] A. Dorfmann, R. Ogden, A pseudo-elastic model for loading, partial unloading and reloading of particle-reinforced rubber, International Journal of Solids and Structures 40 (11) (2003) 2699–2714. doi:10.1016/S0020-7683(03)00089-1.

[46] M. Hossain, P. Steinmann, More hyperelastic models for rubber-like materials: consistent tangent operators and comparative study, Journal of the Mechanical Behavior of Materials 22 (1-2). doi:10.1515/jmbm-2012-0007.

[47] M. Hossain, A. Amin, M. N. Kabir, Eight-chain and full-network models and their modified versions for rubber hyperelasticity: a comparative study, Journal of the Mechanical Behavior of Materials 24 (1-2) (2015) 11 –24. doi:10.1515/jmbm-2015-0002.

[48] A. E. Ehret, On a molecular statistical basis for ogden's model of rubber elasticity, Journal of the Mechanics and Physics of Solids 78 (2015) 249–268. doi:10.1016/j.jmps.2015.02.006.

[49] J. S. Bergstroem, M. C. Boyce, Mechanical behavior of particle filled elastomers, Rubber Chemistry and Technology 72 (4) (1999) 633–656. doi:10.5254/1.3538823.

[50] P. Steinmann, M. Hossain, G. Possart, Hyperelastic models for rubber-like materials: consistent tangent operators and suitability for treloar's data, Archive of Applied Mechanics 82 (9) (2012) 1183–1217. doi:10.1007/s00419-012-0610-z.

[51] L. Mullins, N. R. Tobin, Theoretical model for the elastic behavior of filler-reinforced vulcanized rubbers, Rubber Chemistry and Technology 30 (2) (1957) 555–571. doi:10.5254/1.3542705.

[52] G. Chagnon, On the relevance of continuum damage mechanics as applied to the mullins effect in elastomers, Journal of the Mechanics and Physics of Solids 52 (7) (2004) 1627–1650. doi:10.1016/j.jmps.2003.12.006.

[53] G. Marckmann, E. Verron, L. Gornet, G. Chagnon, P. Charrier, P. Fort, A theory of network alteration for the mullins effect, Journal of the Mechanics and Physics of Solids 50 (9) (2002) 2011–2028. doi:10.1016/s0022-5096(01)00136-3.

[54] A. Dorfmann, R. Ogden, A constitutive model for the mullins effect with permanent set in particle-reinforced rubber, International Journal of Solids and Structures 41 (7) (2004) 1855–1878. doi:10.1016/j.ijsolstr.2003.11.014.

[55] L. Mullins, N. R. Tobin, Stress softening in rubber vulcanizates. part i. use of a strain amplification factor to describe the elastic behavior of filler-reinforced vulcanized rubber, Journal of Applied Polymer Science 9 (9) (1965) 2993–3009. doi:10.1002/app.1965.070090906.